INTERNATIONAL JOURNAL OF HYDROGEN ENERGY 35 (2010) 10381–10386

Available at www.sciencedirect.com

ScienceDirect

journal homepage: www.elsevier.com/locate/he

Hydrogen storage in the iron series of porous Prussian blue analogues

C.P. Krap [a], J. Balmaseda [b], B. Zamora [a], E. Reguera [a,c,*]

[a] Centro de Investigación en Ciencia Aplicada y Tecnología Avanzada del IPN, Unidad Legaria, Mexico
[b] Departamento de Polímeros, Instituto de Investigación en Materiales, UNAM, Mexico
[c] Instituto de Ciencia y Tecnología de Materiales, Universidad de La Habana, 10400 La Habana, Ciudad Habana, Cuba

ARTICLE INFO

Article history:
Received 10 May 2010
Received in revised form
19 July 2010
Accepted 20 July 2010

Keywords:
Prussian blue analogues
Hydrogen storage
Ferricyanides
Hexacyanoferrates(III)

ABSTRACT

The hydrogen storage has been studied in several series of porous Prussian blue analogues but not in the iron one, $T_3[Fe(CN)_6]_2$ with T = Mn, Co, Ni, Cu, Zn, Cd. In this contribution the study of the H_2 adsorption in that series of porous solids is discussed. For comparison, the H_2 adsorption isotherm in $Fe_4[Fe(CN)_6]_3$ was also recorded. All the samples to be studied were characterized from energy-dispersed spectroscopy, X-ray diffraction, infrared, Mössbauer, and thermogravimetric data. The cavity volume to be occupied by the hydrogen molecule was estimated from the amount of water molecules found within the cavity. The obtained value for the cavity volume was then used to calculate the density for the hydrogen storage within the cavity. The obtained density values remain below the value corresponding to its liquid state (71 g/L).

1. Introduction

Hydrogen is being considered an alternative to fossil fuel derivatives as secondary energy bearer for mobile technologies [1,2]; the hydrogen oxidation liberates 142 kJ/g, 3 times the value obtained from gasoline (47.5 kJ/g). Unlike to hydrogen, which can be produced from the water splitting and whose oxidation byproduct is water, fossil fuels derivatives are non-renewable energy sources and their combustion liberates carbon dioxide, which is responsible for the global warming and of the related climate changes. The solar energy accumulated by nature in about 400 millions of years as fossil fuels will be consumed by the human kind in scarcely three centuries [3]. These facts explain the urgency in the hydrogen technology development, particularly for hydrogen production by the water splitting using solar radiation, its storage and then its use through highly efficient and economically viable fuel cell devices. Of these three targets the availability of an appropriate storage method is probably the main challenge [4]. Hydrogen is a small molecule with a low critical temperature ($T_c = 32.97$ K) and above that temperature it is always found in gaseous state. For a pressure of 345 atm, a density of 22 g/L is obtained, relatively low compared to 71 g/L for the liquid state. The storage in liquid state for massive applications appears to be also impractical since the liquefaction process consumes about 40% of the energy to be generated.

Several methods are being studied for hydrogen storage, among them the hydride formation in light weight materials [5,6], high pressure H_2 sequestering within molecular cages (clathrates) [7] and H_2 adsorption in nanoporous solids [8–10]. All these storage methods have limitations and none of them satisfies the established technological requirements [9,11]. The adsorption in nanoporous solids is highly attractive because of the high process reversibility, a feature up to date

* *Corresponding author*. Instituto de Ciencia y Tecnología de Materiales, Universidad de La Habana, 10400 La Habana, Ciudad Habana, Cuba.
E-mail address: ereguera@yahoo.com (E. Reguera).
0360-3199/$ – see front matter
doi:10.1016/j.ijhydene.2010.07.109

not available for the hydride formation, for instance. The H_2 molecule can be adsorbed by means of three types of interactions [12]: (1) dispersive forces resulting from the induction of dipole and quadrupole moments by instantaneous fluctuations in the involved electron clouds; (2) electrostatic forces resulting from the H_2 electron cloud polarization by a charge center, the attractive interaction of the H_2 permanent quadrupole moment with the local electric field gradient, and the one originated by the interaction between quadrupole moments of neighboring H_2 molecules; the first two ones with r^{-4} and r^{-3} dependences, respectively; (3) coordination of the hydrogen molecule to a partially naked transition-metal center. From these facts, porous solids with transition-metal centers located at the surface of the cavities have received a large attention as prototype of materials for H_2 storage [8,9], among them Prussian blue (PB) analogues [13–20]. In anhydrous porous PB analogues always the metal linked at the N end of the CN group is found at the surface of the cavity with an incomplete coordination sphere. In this family of materials all the mentioned adsorption interactions for the H_2 molecule could be present. From the study of the hydrogen adsorption in this family of porous solids valuable information on the involved adsorption forces can be obtained. Within PB analogues, the H_2 adsorption has been well documented for the series $T_3[M(CN)_6]_2$ with T = Mn, Co, Ni, Cu, Zn, Cd; with M = Co, Ir [13–19] but not for M = Fe. In this contribution the recorded H_2 adsorption isotherms in $T_3[Fe(CN)_6]_2$ are discussed. The samples to be studied were characterized from energy-dispersed spectroscopy (EDS), X-ray diffraction (XRD), infrared (IR), Mössbauer, and thermogravimetric (TG) data.

2. Experimental

The samples to be studied were prepared mixing aqueous solutions of $K_3[Fe(CN)_6]$ and sulfate of the involved T^{2+} metals, this last one in a large excess respect to the 2:3 metals (Fe:T) atomic ratio in order to obtain a precipitate free of the alkali metal (K). The formed precipitate was aged for at least two days at room temperature within the mother liqueur and then separated by centrifugation and washed several times with distilled water until to obtain a filtrate free of accompanied ions. The solid was then air dried until it had constant weigh. The PB sample, $Fe_4[Fe(CN)_6]_3 \cdot xH_2O$, was prepared by the same synthetic route. The obtained samples were characterized from EDS, XRD, IR, TG and Mössbauer data.

EDS spectra were recorded using a spectrometer coupled to a Jeol SEM microscopy. IR spectra were run with Perkin–Elmer equipment (Spectrum One model) using the Nujol mulls technique. Metal hexacyanoferrates (III) reduce to hexacyanoferrates (II) when milled and pressed with KBr [21]. XRD powder patterns were obtained with a D8 Advance diffractometer (from Bruker) and CuK_α radiation using secondary monochromator to minimize the fluorescence contribution to the pattern background. Some XRD powder patterns under vacuum and at low temperatures were recorded in the XPD-10B beamline of the LNLS synchrotron radiation facility (Campinas, Brazil). TG curves were collected under a dried nitrogen flow in the high resolution mode using a Q5000 apparatus (from TA Instruments). Mössbauer spectra were obtained at room temperature with a constant acceleration spectrometer operated in the transmission mode and a $^{57}Co/Rh$ source. The recorded Mössbauer spectra were fitted using pseudo-Lorentzian line shape in order to extract the values of isomer shift (δ), quadrupole splitting (Δ), linewidth (Γ) and line area (A, in %).

The H_2 adsorption isotherms were recorded at N_2 liquid temperature using ASAP 2020 analyzer (from Micromeritics). Sample tubes of known weight were loaded with an appropriate amount of sample, ~50 mg, and sealed using TranSeal. In this family of materials, the most reliable adsorption data, using an optimal measurement time, were obtained with a sample of about 50 mg. Previous to recording adsorption isotherms, the samples were degassed on the ASAP analyzer using a heating rate of 5 °C/min and then maintained at the dehydration temperature indicated by the TG curve until a stable outgas rate below 1 μm of Hg was obtained. This process usually requires 24 h of degassing. The degassed sample and sample tube were weighed and then transferred back to the analyzer (with the TranSeal to prevent exposure of the sample to air). After volume measurement with He, the degassing was continued for 24 h at 80 °C in the sample port.

The obtained H_2 adsorption data were fitted using the Osmotic isotherm: [22]

$$P_{eq} = P_{0.5}\left(\frac{n_{ad}}{n_p - n_{ad}}\right)^g \quad (1)$$

where n_{ad} amount adsorbed at the equilibrium pressure P_{eq}, n_p the limiting amount filling the micropores, $P_{0.5}$ is the equilibrium pressure at $n_p/2$ and g is the osmotic coefficient related to ideality of the solution.

The maximum work required to bring a molecule from the adsorbed phase to the gas phase at 800 Torr, A, can be used to compare the adsorbate-adsorbent interactions of the samples studies in volume filling domain corresponding to studied pressures range [22]. It can be calculated by [22]:

$$A = RTg\ln\left(\frac{n_{800}}{n_p - n_{800}}\right) - RTg\ln\left(\frac{n_{ad}}{n_p - n_{ad}}\right) \quad (2)$$

Evaluating Eq. (2) for $P_{eq} = 800$ Torr, clearing the adsorbed quantity (n_{eq}) and substituting in the first term of the work function, the following expression is obtained:

$$A = RT\ln\left(\frac{P_{800}}{P_{0.5}}\right) - RTg\ln\left(\frac{n_{ad}}{n_p - n_{ad}}\right) = RT\ln\left(\frac{P_{800}}{P_{0.5}}\right) - RTg\ln\left(\frac{\theta}{1-\theta}\right) \quad (3)$$

where $\theta = n_{ad}/n_p$ is the volumetric filling.

Eq. (3) reveals that at low volumetric filling, adsorbate–adsorbent interaction is characterized mostly by the value of g, while at volumetric filling of about 0.5 the value of the adsorption work is determined by the magnitude of $P_{0.5}$ parameter.

3. Results and discussion

3.1. Characterization of the samples to be studied

The crystal and electronic structures of the iron series of PB analogues are well documented [23,24] and here only

Table 1 – Unit cell and Mössbauer parameters for the iron series of PB analogues.

Compound	Unit cell parameters, [Å]	Cell contraction on dehydration, [% volume]	Crystallite size, [nm]	Isomer shift (δ), [mm/s][b]	Quadrupole splitting (Δ), [mm/s]
$Mn_3[Fe(CN)_6]_2\cdot 14H_2O$	10.488(1)	5	32	0.11	0.27
$Fe_4[Fe(CN)_6]_3\cdot 16H_2O$	10.167(3)	*	12	0.12	0.00
				0.65	0.59
$Co_3[Fe(CN)_6]_2\cdot 15H_2O$	10.279(1)	4	16	0.12	0.43
$Ni_3[Fe(CN)_6]_2\cdot 16H_2O$	10.204(3)	*	9	0.11	0.50
$Cu_3[Fe(CN)_6]_2\cdot 10H_2O$	10.094(1)	3	21	0.10	0.54
$Zn_3[Fe(CN)_6]_2\cdot 12H_2O$	10.339(1)	6	56	0.12	0.35
$Zn_3[Fe(CN)_6]_2$-R[a]	12.601(1); 32.971(9)	–	*	0.11	0.17
$Cd_3[Fe(CN)_6]_2\cdot 14H_2O$	10.614(1)	5	54	0.11	0.26

* Not measured.
a Rhombohedral phase.
b Fitting errors in δ and Δ remain below 0.01 mm/s.

a summary of their properties is provided. This family of coordination compounds, $T_3[M(CN)_6]_2$, crystallizes with a cubic unit cell related to an octahedral coordination for both inner (M) and outer (T) metals. The cell edge (a) coincides with the T–N≡C–M–C≡N–T chain length. The atomic metals ratio (M:T) senses the amount of vacancies of the octahedral building block, $[M(CN)_6]$, per formula unit; 1/3 for the considered PB analogues series, $T_3[Fe(CN)_6]_2\cdot xH_2O$ [25,26]. PB, $Fe_4[Fe(CN)_6]_3$, has 1/4 of vacancies for the building block. When these vacancies are randomly distributed within the material framework it crystallizes in the Fm-3m space group (T = Mn, Co, Ni, Zn, Cd) where 1/3 of the unit cell volume remains not occupied but, when the vacancies are ordered the crystal structure corresponds to the Pm-3m space (T = Cu) with 50% of free volume [19]. PB and its analogues are usually obtained as fine powders of nanometric crystallite size. For the studied series the crystallite size was estimated from XRD data using the Scherrer equation, resulting, in nm: Mn (32), Fe (12), Co (16), Ni (9), Cu (21), Zn (56), Cd (54) (Table 1). For Ni the XRD powder pattern is formed by relatively broad peaks corresponding to the smallest crystallite size within the series (see Supplementary Information). Fig. 1 shows the porous framework corresponding to the Fm-3m structure. The metal linked at the N end (T) is always found at the surface of the cavities, and with an incomplete coordination sphere. In the as-synthesized material the available coordination positions are occupied by water molecules. The cavity filling is completed by water molecules stabilized through hydrogen bonding interactions with the coordinated ones. On moderate heating both coordinated and hydrogen bonded water molecules evolve preserving the material framework. Fig. 2 shows the TG curves for the considered series, $T_3[Fe(CN)_6]_2\cdot xH_2O$. The temperature of dehydration

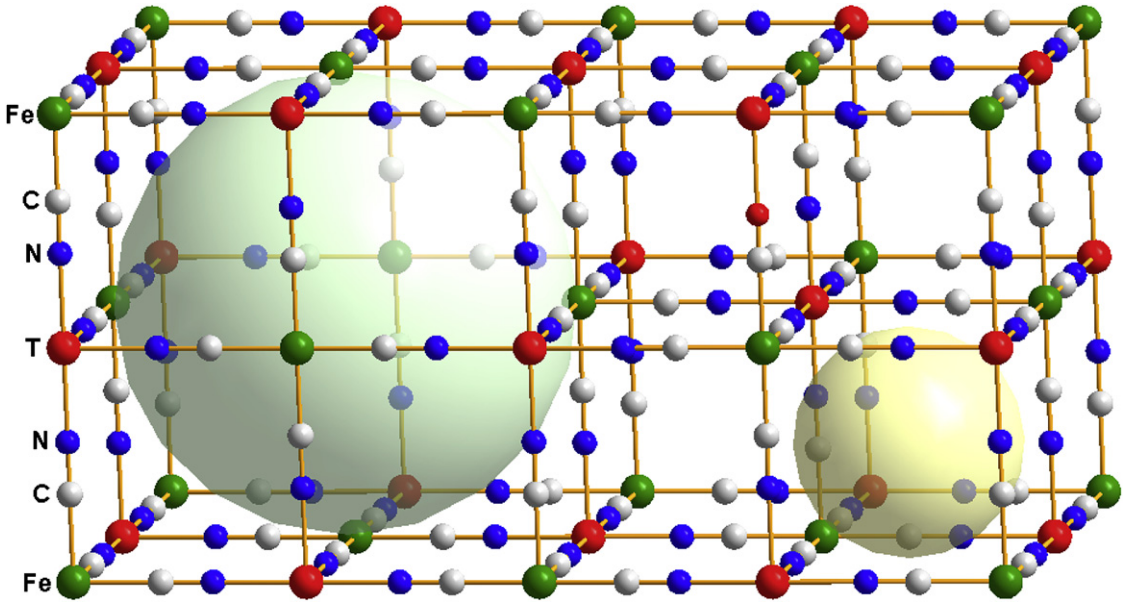

Fig. 1 – Porous framework for the studied series of Prussian blue analogues. The larger sphere represents a cavity related to a vacancy of the building block, $[Fe(CN)_6]$. The smaller sphere represents a free interstitial space.

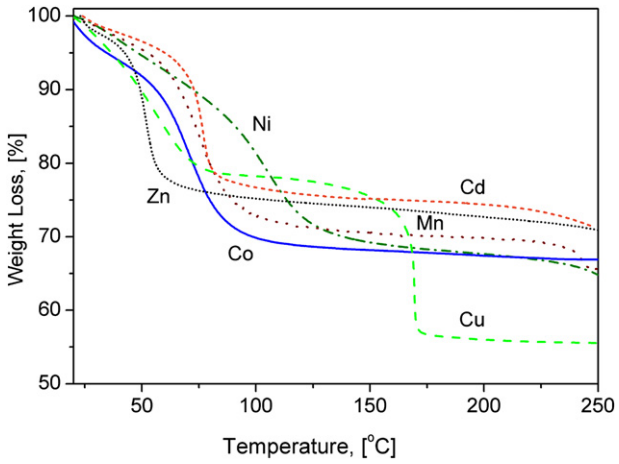

Fig. 2 – TG curves for the iron series of Prussian blue analogues. All the compounds become anhydrous for a moderate heating below 100 °C except for Ni which requires a higher temperature. The lowest dehydration temperatures are observed for Zn and Cu.

follows the order Ni > Co > Mn > Cd > Cu > Zn, and it senses the metal polarizing power and the strength of its electrostatic interaction with the water molecule. For Zn the crystal water removal on heating leads to a structural transition to a rhombohedral phase where the Zn atom is found with a tetrahedral coordination to N ends of the CN groups. The behavior of PB samples on heating has been reported [27]. The presence of iron (III) atoms at the surface of cavities in PB leads to a relatively strong surface interaction with the water molecules and from this fact to obtain anhydrous PB samples relatively high temperatures (>150 °C) or large heating times (>12 h) are required.

The electronic structure of the materials under study can be sensed from Mössbauer and IR spectra [23,24,26]. Their Mössbauer spectra are quadrupole splitting doublets with isomer shift (δ) values about 0.11 mm/s (relative to sodium nitroprusside) (see Table 1). These δ values are typical of low spin ferric ions, an expected result since the CN group at the C end behaves as a strong ligand. Once the water molecules are removed, the metal T only interacts with the framework ligands increasing the amount of electron density subtracted from the CN group via its 5σ orbital. This enhances the π-back donation at the C end reducing the 3*d* electron density at the iron atom sensed as a down shift in the value of δ. In the XRD powder pattern it is observed as a reduction for the T–N≡C–Fe–C≡N–T chain length, for a unit cell volume reduction in the 2–6% range (Table 1). The ν(CN) stretching frequency is observed in the 2186–2152 cm^{-1} range: Mn (2167), Co (2186), Ni (2166), Cu (2174), Zn (2161), Cd (2152). For PB the ν(CN) vibration is observed at 2080 cm^{-1}, a frequency value characteristic of a hexacyanoferrates (II). That vibration in PB analogues senses the metal–ligand interactions at both the C and N ends of the CN group.

3.2. *Adsorption isotherms*

The accessibility of the porous framework of the studied series of solids to small molecules, like CO_2, N_2 and H_2O, is known from a previous adsorption study [23]. In porous PB analogues all the crystal water is found occupying the larger cavity (Fig. 1). The interstitial spaces remain free of water molecules. The platinum series, T[Pt(CN)$_6$], which is free of vacancies forms anhydrous solids [28]. Similar behavior has also been observed for the H_2 adsorption; the hydrogen molecule is not adsorbed in the interstitial spaces [17,18]. From these facts, the cavity volume where the hydrogen molecule is adsorbed was estimated from the amount of water molecules within the cavity, considering that they are in a highly condensed state, 1 kg/L (the density of water at 4 °C). The obtained values for the cavity volume are summarized in Table 2.

Fig. 3 shows the recorded H_2 adsorption isotherms in the iron series of PB analogues. These isotherms show an abrupt slope in the low pressure region and then certain trend to saturation is appreciated. Such behavior is typical of presence of a relatively strong adsorption interaction for the hydrogen molecule. The isotherm slope at low pressures senses the strength for the guest-host interaction. These isotherms were fitted using the Osmotic model, Eq. (1), in order to estimate the limit adsorption for $P \rightarrow \propto$, and the value for the osmotic parameter (g) as sensor for the strength of the involved adsorption forces. In Table 2 the obtained values for the parameters model are collected. The low amount of H_2 adsorbed for PB was attributed to occurrence of partial decomposition in that compound related to its small crystallite size (12 nm) (Table 1) and also to the high heating temperature required to remove the water molecules that occupy the cavity volume. The adsorption isotherm obtained for Ni does not corresponds to a nanoporous solid, suggesting that the porous framework has collapsed during the required prolonged activation and degassing processes (48 h of heating under vacuum), which for the case of Ni also involves the

Table 2 – Results from the H_2 adsorption isotherms fitted according to the Osmotic model (Eq. (1)).

Sample	n_p [mol/mol]	n_p [wt%]	Cavity volume [Å^3]	H_2/cavity	ρ (g/L)	g
$Mn_3[Fe(CN)_6]_2$	6.9 ± 0.2	2.33	419	6.9	55	1.47 ± 0.04
$Fe_4[Fe(CN)_6]_3$	2.7 ± 0.2	0.93	478	2.7	20	1.86 ± 0.19
$Co_3[Fe(CN)_6]_2$	6.7 ± 0.3	1.86	449	6.7	47	1.60 ± 0.10
$Cu_3[Fe(CN)_6]_2$	5.5 ± 0.4	1.79	419	5.5	44	1.61 ± 0.09
$Zn_3[Fe(CN)_6]_2$	5.7 ± 0.1	1.86	419	5.7	46	1.41 ± 0.05
$Cd_3[Fe(CN)_6]_2$	7.7 ± 0.2	2.01	469	7.7	55	1.52 ± 0.06

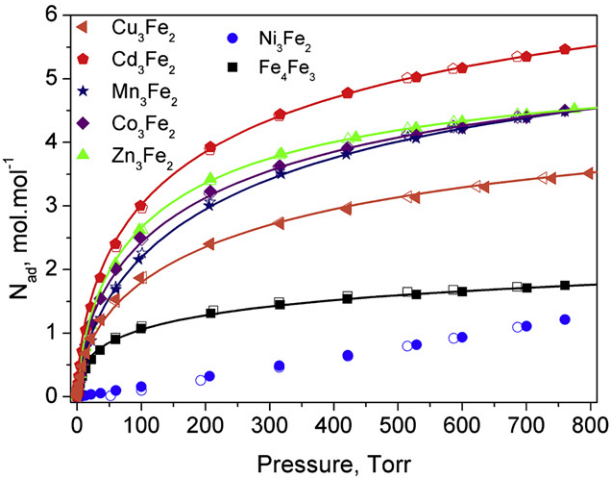

Fig. 3 – H_2 adsorption isotherms recorded at N_2 liquid temperature for the iron series of Prussian blue analogues.

highest heating temperature within the series (Fig. 2). The low thermal stability of the Ni containing composition is additionally favored by its small crystallite size (9 nm), the smallest one within the series.

The adsorption work dependence on the volumetric filling was evaluated according to Eq. (3). The order of the adsorption work for the low volume filling region results Fe > Cu ~ Co > Cd > Mn ~ Zn (Fig. 4, inset). That order is similar to that found from the value for the osmotic parameter (*g*) (Table 2). Such behavior finds explanation in the specific interaction between the metal found at the surface of the cavities with the hydrogen molecule. In PB, $Fe_4[Fe(CN)_6]_3$, the trivalent state for the iron atom favors a relatively strong electrostatic interaction with the hydrogen molecule (polarization of the H_2 electron cloud and through its quadrupole moment). The weak interaction observed for Zn, the weakest one in the series, is related to the tetrahedral coordination for this metal in the rhombohedral phase, which hinders a direct

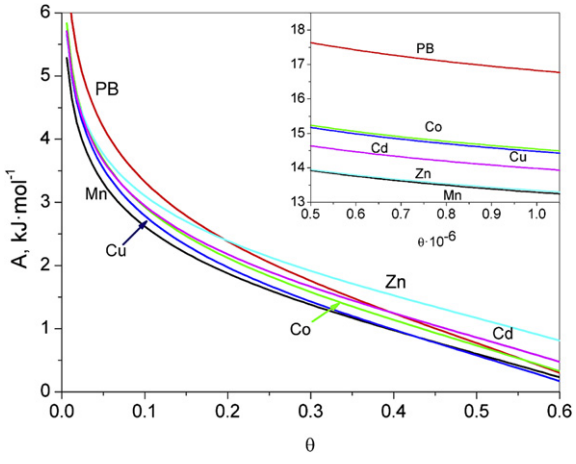

Fig. 4 – The maximum work required to bring a molecule from the adsorbed phase to the gas phase at 800 Torr in experimental volume filling domain. Inset: low volumetric filling region. The stronger guest–host interaction was observed for PB.

metal-H_2 interaction. In this case the adsorption forces are related to the existence of certain electric field gradient close to the cavity windows and its interaction with the H_2 quadrupole moment with also certain contribution from dispersive forces. In porous PB analogues the copper atom shows a unique behavior, with a relatively low effective charge and, in consequence, with a weak electrostatic interaction with water molecules (see Fig. 2) and also with the hydrogen ones. However, such low effective valence is a favorable feature for its coordination interaction with H_2, possibility not available for the remaining metals of this series. This explains the relatively strong adsorption interaction for copper containing PB analogues [17]. The coordination interaction requires of the metal and H_2 orbitals overlapping and from this fact it is a short distance interaction, which allows the adsorption of only one layer of H_2 molecules in the metal environment. In the presence of a strong charge center the H_2 adsorption in multilayers could be possible because of the r^{-3} and r^{-4} dependence of the resulting electrostatic interactions. It seems the charge center found at the surface of the cavity for PB analogues is not enough to allow high density H_2 storage (discussed below).

According to the metals polarizing power, for Co, Mn and Cd, the expected order for the adsorption forces strength is Co > Mn > Cd. The relatively stronger interaction observed for Cd, relative to Mn, could be attributed to the contribution of dispersive forces, favored by the dense electron cloud of the Cd atom. The dispersive interaction enhances when the electron density of the involved interacting species increases since more intense dipole moments are induced by fluctuations of the electron clouds.

The observed order for the limit adsorption capacity, in mol/mol, for the iron series of PB analogues (Table 2), Cd > Mn > Co > Zn > Cu is quite different from that found for cobalt and iridium series [18], Cu > Zn > Co > Cd > Mn. Such difference of behavior can be attributed to a different thermal stability for these series of PB analogues. For some metals in the iron series, e.g. Cu, relatively low thermal stability is observed (Fig. 2). From the obtained value of H_2 molecules adsorbed per cavity and the calculated cavity volume, the density of H_2 storage was estimated (Table 2). Without exception, all the obtained value for $\rho(H_2)$ remains below the H_2 density in liquid state, 71 g/L. The same behavior is observed when the values for $\rho(H_2)$ in the cobalt series are calculated from the reported H_2 adsorption data [13]. This suggests that the electrostatic adsorption potential within the cavity of PB analogues is insufficient to allow a high H_2 storage density. In porous PB analogues the effective charge on the metal found at the cavity surface is significantly reduced by electron density donation from the framework CN ligand. Such effect is appreciate from magnetic and Mössbauer data for iron series of PB analogues [26].

4. Conclusions

The hydrogen storage in the iron series of PB analogues was studied. On the prolonged heating required for hydrogen adsorption studies in porous solids, for some metals of this series, among then Ni and Cu, and PB, at least partial

decomposition is observed reducing the H_2 storage capacity. However, the specific interaction of the hydrogen molecule with the metal found at the surface of the cavities for the sample fraction that remains stable is not affected. The observed strength for the adsorption forces, sensed through the value of the osmotic parameter, g, and the adsorption work (A) for low volumetric filling, finds explanation in the expected specific interaction of the hydrogen molecule with the partially naked metal; except for Cu and Cd, it is dominated by the electrostatic interactions. Such behavior coincides with that already observed behavior for cobalt and iridium series. The estimated density for the H_2 storage in the iron series of PB analogues remains below the value for liquid hydrogen.

Acknowledgement

This study was partially supported by the Projects ICyTDF-PIFUTP08-158 and SEP-CONACyT 2009-123480. The authors thank the access to the LNLS synchrotron radiation facility to obtain information on the materials structural stability under cryogenic conditions.

Appendix A. Supplementary data

Supplementary data associated with this article can be found, in the online version, at doi:10.1016/j.ijhydene.2010.07.109.

REFERENCES

[1] Schlapbach L, Züttel A. Hydrogen-storage materials for mobile applications. Nature 2001;414:353–8. and references therein.
[2] Barreto L, Makihira A, Riahi K. The hydrogen economy in the 21st century: a sustainable development scenario. Int J Hydrogen Energy 2003;28:267–84.
[3] Dunn S. Hydrogen futures: toward a sustainable energy system. Int J Hydrogen Energy 2002;27:235–64.
[4] Ball M, Wietschel M. The future of hydrogen – opportunities and challenges. Int J Hydrogen Energy 2009;34:615–27.
[5] Orimo S-I, Nakamori Y, Eliseo JR, Züttel A, Jensen CM. Complex hydrides for hydrogen storage. Chem Rev 2007;107:4111–32.
[6] Xiong Z, Yong CK, Wu G, Chen P, Shaw W, Karkamkar A, et al. High-capacity hydrogen storage in lithium and sodium amidoboranes. Nature Mater 2008;7:138–41.
[7] Struzhkin VV, Militzer B, Mao WL, Mao H-K, Hemley RJ. Hydrogen storage in molecular clathrates. Chem Rev 2007;107:4133–51.
[8] Bhatia SK, Myers AL. Optimum conditions for adsorptive storage. Langmuir 2006;22:1688–700.
[9] Liu Y, Kabbour H, Brown CM, Neumann DA, Ahn CC. Increasing the density of adsorbed hydrogen with coordinatively unsaturated metal centers in metal–organic frameworks. Langmuir 2008;24:4772–7.
[10] Li Y, Liu Y, Wang Y, Leng Y, Xie L, Li X. Hydrogen storage properties of [M (Py){Ni (CN)4}] (M=Fe, Co, Ni). Int J Hydrogen Energy 2007;32:3411–5.
[11] <http://www.energy.gov/energysources/hydrogen.htm>.
[12] Reguera E. Materials for hydrogen storage in nanocavities: design criteria. Int J Hydrogen Energy 2009;34:9163–7.
[13] Kaye SS, Long JR. Hydrogen storage in the dehydrated Prussian blue analogues $M_3[Co(CN)_6]_2$ (M = Mn, Fe, Co, Ni, Cu, Zn). J Am Chem Soc 2005;127:6506–7.
[14] Chapman KW, Southon PD, Weeks CL, Kepert CJ. Reversible hydrogen gas uptake in nanoporous Prussian Blue analogues. Chem Commun; 2005:3322–4.
[15] Kaye SS, Long JR. The role of vacancies in the hydrogen storage properties of Prussian blue analogues. Catal Today 2007;120:311–6.
[16] Natesakhawat S, Culp JT, Matranga C, Bockrath B. Adsorption properties of hydrogen and carbon dioxide in Prussian blue analogues $M_3[Co(CN)_6]_2$, (M = Co, Zn). J Phys Chem C 2007;111:1055–60.
[17] Reguera L, Krap CP, Balmaseda J, Reguera E. Hydrogen storage in copper Prussian blue analogues: evidence of H_2 coordination to the copper atom. J Phys Chem C 2008;112:15,893–15,899.
[18] Krap CP, Balmaseda J, del Castillo LF, Zamora B, Reguera E. Hydrogen storage in Prussian Blue analogues: H_2 interaction with the metal found at the cavity surface. Energy Fuels 2010;24:581–9.
[19] Jiménez-Gallegos J, Rodríguez-Hernández J, Yee-Madeira H, Reguera E. Structure of porous copper Prussian Blue analogues: nature of their high H_2 storage capacity. J Phys Chem C 2010;114:5043–8.
[20] Yuan A-H, Chu C-X, Zhou H, Yuan P, Liu K-K, Li L, et al. Syntheses, crystal structures and gas sorption properties of Prussian blue analogues constructed from [Cr(CN)6]3– building blocks. Eur J Inorg Chem 2010;6:866–71.
[21] Fernández-Bertrán J, Reguera E. Mechanochemical reactions in alkali halide pressed disks. Solid State Ionics 1997;93:139–46.
[22] Bering BP, Serpinskii VV. Osmotic theory of adsorption equilibrium. Izv Akad Nauk SSSR, Ser Xim 1974;11:2427–51.
[23] Balmaseda J, Reguera E, Rodríguez-Hernández J, Reguera L, Autie M. Behavior of transition metals ferricyanides as microporous materials. Micropor Mesopor Mater 2006;96:222–36.
[24] Martínez-García R, Knobel M, Reguera E. Thermal-induced changes in molecular magnets based on Prussian blue analogues. J Phys Chem B 2006;110:7296–303.
[25] Ludi A, Gudel HU. Structural chemistry of polynuclear transition metal cyanides. Struct Bond 1973;14:1–21.
[26] Martínez-García R, Knobel M, Reguera E. Modification of the magnetic properties in molecular magnets based on Prussian blue analogues through adsorbed species. J Phys Condens Matter 2006;18:11243–54.
[27] Bennett MV, Beauvais LG, Shores MP, Long JR. Expanded Prussian blue analogues incorporating $[Re_6Se_8(CN)_6]^{3-/4-}$ clusters: adjusting porosity via charge balance. J. Am. Chem. Soc. 2001;123:8022–34.
[28] Babkov AV, Kharitonov YuYa. Hexacyanoplatinates (IV) and Hexacyanopalladates (IV). Russ J Inorg Chem 1999;44:1749–63.